

# Moiré pattern multiplicity driven by electronic effects in two-dimensional $\text{CrCl}_3/\text{Au}$ heterostructures.

Eugenio Gambari,<sup>†</sup> Hugo Le Du,<sup>†</sup> Mathieu Lizée,<sup>‡</sup> Arindam Mukherjee,<sup>†</sup> Laurent Limot,<sup>¶</sup> Fabrice Scheurer,<sup>¶</sup> Marie D'angelo,<sup>†</sup> François Debontridder,<sup>†</sup> Tristan Cren,<sup>†</sup> and Marie Hervé\*,<sup>†</sup>

<sup>†</sup>*Sorbonne Université, CNRS, Institut des Nanosciences de Paris, UMR7588, 4 place Jussieu, Paris, 75005, France*

<sup>‡</sup>*Fritz Haber Institute of the Max Planck Society, Berlin, Germany*

<sup>¶</sup>*Université de Strasbourg, CNRS, Institut de Physique et Chimie des Matériaux de Strasbourg, UMR7504, Strasbourg, F-67000, France*

E-mail: marie.herve@sorbonne-universite.fr

## Abstract

Moiré patterns are a central motif in van der Waals heterostructures arising from the superposition of two-dimensional (2D) incommensurate lattices. These patterns reveal a wealth of correlated effects, influencing electronic, magnetic, and structural phenomena. While diffraction techniques typically resolve multiple moiré wave-vectors corresponding to the incommensurate nature of the underlying lattices, Scanning Tunneling Microscopy (STM) often reveals only a dominant superperiod. In this work, we address this apparent discrepancy through an STM study of a twisted monolayer of  $\text{CrCl}_3$  on  $\text{Au}(111)$ . We observe the coexistence of several moiré patterns at a fixed twist

angle, whose relative intensity depends on the tunneling bias. Fourier analysis of STM data uncovers hidden higher-order moiré components not visible in STM topographic images, while spectroscopy maps reveal that the spectral weight of each pattern varies with electron energy. Our results establish that STM selectively probes on the same area distinct moiré modulations depending on electronic confinement, providing a unified framework that reconciles real space and reciprocal space observations of complex moiré superstructures.

## Introduction

Moiré patterns in two-dimensional materials are ubiquitous. They are found in van der Waals heterostructures such as Gr/Ir, Gr/Pt,<sup>1–5</sup> MoS<sub>2</sub>/Au<sup>6,7</sup> when the lattice parameters of the two materials are incommensurate, or in twisted bilayers of van der Waals materials such as graphene, CrI<sub>3</sub>, or WSe<sub>2</sub>.<sup>5,8–16</sup> For specific orientations, moiré patterns can lead to the emergence of flat bands<sup>17,18</sup> giving rise to many exciting physical phenomena. Recently, superconductivity has been discovered in materials that are not intrinsically superconducting, such as twisted bilayer graphene or WSe<sub>2</sub>.<sup>10,14</sup> Wigner crystals have been observed in moiré lattices of WSe<sub>2</sub>/WS<sub>2</sub>.<sup>16</sup> Non-collinear magnetic orders have been reported in materials in which they are usually collinear, such as in twisted bilayers of CrI<sub>3</sub>.<sup>11–13</sup>

Moiré patterns are a direct manifestation of the quasiperiodic structure induced by the superposition of two incommensurate periodic lattices. In reciprocal space this leads to an infinite number of satellite peaks surrounding the Bragg peaks, as observed by diffraction techniques.<sup>2,7,19</sup> However, other experimental probes accessing to the real space order, such as scanning probe microscopy techniques, tend to reveal a single dominant moiré pattern that is commonly interpreted as a commensurate superperiod.<sup>20–25</sup>

The use of a periodic superlattice description in *ab-initio* calculations is also quite common. For example this is used for the prediction of a periodic non-collinear magnetic order in twisted bilayers of CrI<sub>3</sub>.<sup>26</sup> It sometimes happens that the same system studied by diffrac-

tion and STM leads to contradictory observations, as in the case of MoS<sub>2</sub>/Au.<sup>7</sup> The two approaches, in real and reciprocal space, seem to differ conceptually. In this paper, we link them through a real space study exhibiting the coexistence of several moiré patterns in a same location. In particular, our analysis reveals that STM is selectively sensitive to different coexisting moiré patterns, depending on the energy of the probed electrons.

When examining a moiré pattern arising from the superposition of two 2-dimensional periodic lattices, as observed in van der Waals heterostructures, the mathematical representation of the moiré pattern in real space can become quite complex, especially when higher-order moiré patterns are involved.<sup>1-3,5,8,19,27</sup> In contrast, the description in reciprocal space is quite straightforward,<sup>1,8,28</sup> a moiré pattern is generated when two periodic functions with spatial frequencies  $\mathbf{Q}_1$  and  $\mathbf{Q}_2$  are multiplied together. This yields a beating frequency  $\mathbf{Q}_{\text{moiré}} = \mathbf{Q}_1 - \mathbf{Q}_2$ , corresponding to the moiré wave vector. For two 2-dimensional atomic lattices, the general reciprocal lattice vectors of lattice 1 and 2,  $\mathbf{Q}_1^{i,j}$  and  $\mathbf{Q}_2^{k,l}$  can be expressed as linear combinations of the primitive reciprocal lattice vectors  $\mathbf{Q}_1^{1,0}$ ,  $\mathbf{Q}_1^{0,1}$ ,  $\mathbf{Q}_2^{1,0}$  and  $\mathbf{Q}_2^{0,1}$ , as:

$$\mathbf{Q}_1^{i,j} = i\mathbf{Q}_1^{1,0} + j\mathbf{Q}_1^{0,1} \quad \mathbf{Q}_2^{k,l} = k\mathbf{Q}_2^{1,0} + l\mathbf{Q}_2^{0,1} \quad (1)$$

This leads to an infinite number of possible Fourier components of the moiré patterns, where the wave vectors can be expressed as:

$$\mathbf{Q}_{\text{moiré}}^{i,j,k,l} = \mathbf{Q}_1^{i,j} - \mathbf{Q}_2^{k,l} \quad (2)$$

Electron diffraction experiments often reveal multiple moiré patterns in the Fourier space for a given specific orientation between the atomic lattices<sup>2,7,19</sup> whereas STM experiments often identify a single dominant moiré pattern.<sup>2,7</sup> A possible reason for that could be that electron diffraction integrate over large surface areas while STM reveal a local order. Pham et al.<sup>22</sup> showed that the moiré contrast observed in STM topographs depends on the tunneling

bias, suggesting that the modulation is electronic rather than structural. However, STM topography alone are not straightforward to interpret in real space since several distinct moiré modulations may coexist at the same energy and within the same real-space region, with often one dominant component that hides less intense modulations. We will show that an efficient way to reveal the coexistence of multiple moiré patterns consist in combining energy-resolved spectroscopy with Fourier-space analysis. Here, we study a  $\text{CrCl}_3$  monolayer on  $\text{Au}(111)$  and show that the moiré landscape is far richer than what topography alone reveals. Fourier analysis of STM data uncovers hidden higher-order moiré components not visible in STM topographic images, while spectroscopy maps reveal that the spectral weight of each pattern varies with electron energy. Our results establish that STM selectively probes on a same area distinct moiré modulations depending on electronic confinement. These findings provide a unified framework for complex moiré superstructures, and, more generally, imply that the emergent electronic, magnetic, and correlated properties of moiré materials cannot be fully understood within a single-period description.

## Results and discussion

$\text{CrCl}_3$  monolayer islands were grown on a clean  $\text{Au}(111)$  substrate by molecular beam epitaxy (MBE).<sup>8</sup> Figure 1a displays a large-scale STM topography of the surface. The bare atomic terraces of the  $\text{Au}(111)$  substrate are partially covered by  $\text{CrCl}_3$  monolayer islands, presenting a width larger than 100 nm. These islands can grow with various crystalline orientations with respect to the  $\text{Au}(111)$  surface, leading to the formation of different moiré patterns (see Supporting Information S1). We can sort the island orientations into two main sets, labeled as  $\alpha$  and  $\beta$ . The dense crystallographic directions of the  $\text{CrCl}_3^\alpha$  islands (Figure 1a) are aligned with those of the underlying  $\text{Au}(111)$  lattice ( $\langle 1\bar{1}0 \rangle_{\text{Au}}$ ), while the  $\text{CrCl}_3^\beta$  islands (Figure 1b) are twisted by about  $30^\circ$ . In the  $\text{CrCl}_3^\alpha$  islands, a dominant moiré pattern with a periodicity of 6.2 nm is observed (Figure 1a). By contrast, a much shorter periodicity of approximately

1.6 nm is observed in  $\text{CrCl}_3^\beta$  islands (Figure 1b). In a prior study, we conducted a detailed analysis of the moiré pattern and the associated topological defects found in the  $\text{CrCl}_3^\alpha$  islands.<sup>8</sup> In the present work, we focus on the  $\text{CrCl}_3^\beta$  islands, showing that the observed superstructure stems from the superposition of multiple moiré patterns. Figure 2 shows a detailed analysis of the moiré patterns in  $\text{CrCl}_3^\beta$  islands. The crystallographic orientation of these domains varies slightly from island to island, between about  $30^\circ$  and  $35^\circ$  relative to the  $\langle 1\bar{1}0 \rangle_{\text{Au}}$  direction. Two limiting cases are shown in Figures 2a and 2b: one island showing a  $30^\circ$  twist and the other a  $35^\circ$  one. For these configurations, as well as for intermediate angles, the observed superstructures arise from the superposition of multiple moiré patterns, as revealed by reciprocal space analysis. Figures 2c and 2d are obtained by performing the 2D Fourier Transform (FT) of the STM topographies in Figures 2a and 2b, respectively.

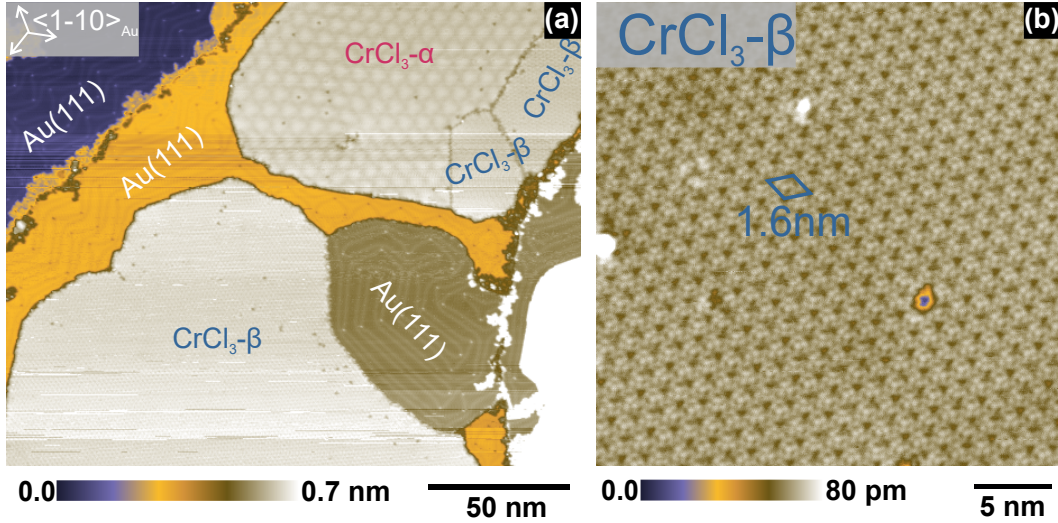


**Fig. 1.** STM topography of  $\text{CrCl}_3$  islands deposited on  $\text{Au}(111)$ . (a) Large scale STM topography displaying the two types of  $\text{CrCl}_3$  islands:  $\text{CrCl}_3^\alpha$  and  $\text{CrCl}_3^\beta$ . Their atomic lattices are twisted by  $30^\circ$  with respect to each other and their surfaces show two distinct moiré patterns. (b) STM topography of a  $\text{CrCl}_3^\beta$  island, the moiré pattern has a periodicity of 1.6 nm. Tunneling parameters: (a)  $V = 1.2$  V,  $I = 100$  pA; (b)  $V = 1.4$  V,  $I = 100$  pA.

These FT images reveal numerous spots. Figures 2e and 2f present the same Fourier-transform images as in Figures 2c and 2d, with Bragg spots and moiré satellites highlighted. Red circles indicate the main Bragg spots corresponding to the dense atomic directions of  $\text{CrCl}_3$ , while black circles denote higher-order Bragg spots rotated by  $30^\circ$  relative to the dense

atomic axes. The remaining spots correspond to satellites from multiple moiré patterns. The superposition of the  $\text{CrCl}_3$  and  $\text{Au}(111)$  hexagonal lattices generates a hexagonal moiré superlattice in real space, which manifests in reciprocal space as six satellite spots forming a hexagon around each  $\text{CrCl}_3$  Bragg peak. In Figure 2e, where the  $\text{CrCl}_3$  lattice is twisted by  $30^\circ$  relative to  $\langle 1\bar{1}0 \rangle_{\text{Au}}$ , three moiré patterns (highlighted by green, red, and black hexagons) are visible both at the Brillouin zone center and around the Bragg peaks. For a domain twisted by  $35^\circ$  (Figure 2f), four distinct moiré patterns appear, marked by orange, pink, green, and red hexagons. Each vertex of the moiré hexagons in the FT images originates from the conjunction of one  $\text{CrCl}_3$  and one  $\text{Au}(111)$  Bragg spot, denoted  $(i,j)_{\text{CrCl}_3}$  and  $(k,l)_{\text{Au}}$ . To identify which Bragg spots generate a given moiré component, we superimposed the reciprocal lattices of  $\text{CrCl}_3$  (violet) and  $\text{Au}(111)$  (blue), as shown in Figures 2g and 2h. In Figure 2g, the  $\text{CrCl}_3$  lattice is twisted by  $30^\circ$  relative to  $\langle 1\bar{1}0 \rangle_{\text{Au}}$ , and by  $35^\circ$  in Figure 2h. This angular relationship is illustrated by the brown dashed arrows indicating the  $\mathbf{Q}_{\text{Au}}^{1,0}$  and  $\mathbf{Q}_{\text{CrCl}_3}^{1,0}$  directions. For clarity, only one quadrant of reciprocal space is shown; the complete construction is provided in the Supporting Information S2. By measuring the size and orientation of a given  $\mathbf{Q}_{\text{moiré}}$  in Figures 2e and 2f, we can determine which pair of Bragg vectors, from Au and  $\text{CrCl}_3$ , is involved. As highlighted by green hexagons in Figures 2e and 2f, the dominant moiré pattern arises from the same combination of  $\text{Au}(111)$  and  $\text{CrCl}_3$  lattice vectors, although its size and orientation differ between the two domains. In the  $30^\circ$  twisted domain (Figure 2e), the green highlighted moiré spots are aligned with the higher order  $\text{CrCl}_3$  Bragg spots (marked by black circles). The associated  $\mathbf{Q}_{\text{moiré}}$  is shown as a green arrow in Figure 2g and is oriented at  $30^\circ$  from  $\mathbf{Q}_{\text{CrCl}_3}^{1,0}$ . In the  $35^\circ$  domain (Figure 2f), the same moiré spots line up with the first order Bragg spots marked by the red circles, and the corresponding  $\mathbf{Q}_{\text{moiré}}$  (the green arrow in Figure 2h) lies parallel to  $\mathbf{Q}_{\text{CrCl}_3}^{1,0}$ . We found that the dominant moiré present in these twisted domains correspond to the conjunction of the  $(2,1)_{\text{CrCl}_3}$  and  $(1,1)_{\text{Au}}$  spots. The graphical constructions in Figures 2e and 2f illustrate that a  $5^\circ$  twist of the  $\text{CrCl}_3$  lattice results in an approximately  $30^\circ$  rotation of the two moiré

patterns. By analyzing in this manner all moiré patterns observed in the  $30^\circ$  and  $35^\circ$  twisted domains, we identified three and four pairs of Bragg spots, respectively, as indicated by the colored arrows in Figures 2g and 2h. The corresponding Bragg spots are listed in Table 1.

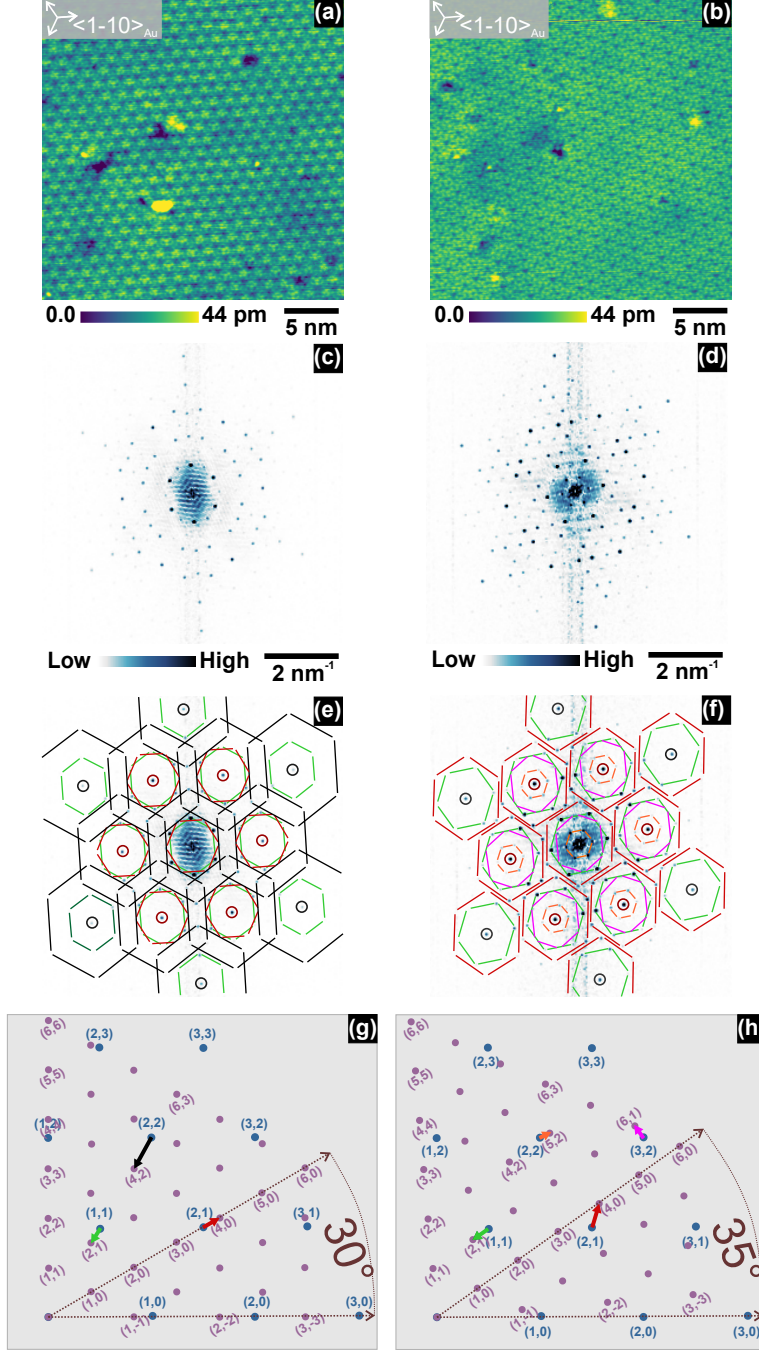


**Fig. 2.** Analysis of multiple moiré patterns observed in  $\text{CrCl}_3^\beta$  islands. (a),(b) STM topographies of  $\beta$  islands with atomic lattices rotated by  $30^\circ$  and  $35^\circ$  relative to the  $\langle 1\bar{1}0 \rangle_{\text{Au}}$  direction. Tunneling parameters:  $V = 1.5 \text{ V}$ ,  $I = 100 \text{ pA}$ . (c),(d) Corresponding Fourier transform images. (e),(f) Same FT images as in (c),(d), with highlighted Bragg spots: the  $\text{CrCl}_3$  spots are marked by red and black circles, while the moiré spots are located at the vertices of colored hexagons. (g),(h) Graphical constructions of the  $\text{CrCl}_3$  (violet) and Au (blue) reciprocal lattices for twist angles of  $30^\circ$  and  $35^\circ$ . Colored arrows indicate the Bragg spot pairs responsible for the distinct moiré patterns.



**Table 1.** Summary of  $\text{CrCl}_3$  and Au Bragg spot pairs generating different moiré components in  $30^\circ$  and  $35^\circ$  twisted domains.

Twist angle	Green (2,1) $_{\text{CrCl}_3}$ /(1,1) $_{\text{Au}}$	Black (2,1) $_{\text{CrCl}_3}$ /(1,1) $_{\text{Au}}$	Red (4,0) $_{\text{CrCl}_3}$ /(2,1) $_{\text{Au}}$	Orange (5,2) $_{\text{CrCl}_3}$ /(2,2) $_{\text{Au}}$	Pink (6,1) $_{\text{CrCl}_3}$ /(3,2) $_{\text{Au}}$
$30^\circ$	Detected	Detected	Detected	Not detected	Not detected
$35^\circ$	Detected	Not detected	Detected	Detected	Detected

Slight variations in the orientation of  $\text{CrCl}_3$  lead to the appearance or disappearance of specific moiré patterns. For example, the moiré marked in black in Figure 2e, resulting from the conjunction of  $(4,2)_{\text{CrCl}_3}$  and  $(2,2)_{\text{Au}}$ , disappears when the  $\text{CrCl}_3$  lattice is twisted from  $30^\circ$  to  $35^\circ$ . In the  $35^\circ$  domain (Figure 2f), two additional moiré patterns emerge (in orange and pink) and originate from the pairs  $(5,2)_{\text{CrCl}_3}/(2,2)_{\text{Au}}$  and  $(6,1)_{\text{CrCl}_3}/(3,2)_{\text{Au}}$  respectively. For both orientations of  $\text{CrCl}_3$  presented in Figure 2, the various overlapping moiré patterns have similar periodicities, making them challenging to distinguish in real space images. The topographic contrast in Figures 2a and 2b is dominated by a moiré stemming from the  $(2,1)_{\text{CrCl}_3}$  and  $(1,1)_{\text{Au}}$  conjunction (the green arrows in Figures 2g and 2h). For these two twist angles, disentangling the contributions of overlapping moiré patterns requires reciprocal space analysis, as shown in Figures 2e and 2f.

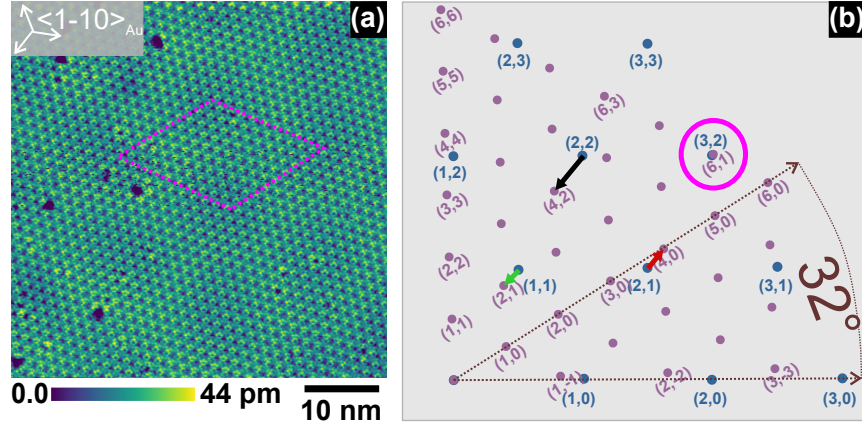


**Fig. 3.** (a) STM topography of a  $\text{CrCl}_3^\beta$  island twisted of approximately  $32^\circ$  relative to the  $\langle 1\bar{1}0 \rangle_{\text{Au}}$  direction, showing a weak, long-wavelength moiré modulation ( $\sim 20$  nm) superimposed on the dominant  $\sim 1.6$  nm moiré pattern. Tunneling parameters:  $V = 1.2$  V,  $I = 100$  pA. (b) Graphical construction of  $\text{CrCl}_3$  and Au reciprocal lattices. The Bragg spot pair generating the longer period moiré is circled in pink.

At intermediate twist angles, such as  $32^\circ$ , the Bragg spots associated with the pink moiré,  $(6,1)_{\text{CrCl}_3}$  and  $(3,2)_{\text{Au}}$ , approach one another in reciprocal space (see Figure 3b). As a consequence, the corresponding moiré wave vector becomes so small that its spots are buried within the central region of the FT, where background contributions from other electronic structure effects dominate. In real space, this moiré manifests as a long-wavelength modulation, clearly distinguishable from the shorter-period moirés, despite its comparatively weak spectral weight. Figure 3a shows an STM topography of a region where the  $\text{CrCl}_3$  lattice is twisted by approximately  $32^\circ$ . Alongside the main moiré modulation, with a real-space period of about 1.6 nm, a fainter superstructure with a larger period of approximately 20 nm is also observed.

We now show that the observed moiré patterns originate from electronic effects rather than from any modulation of the out-of-plane atomic positions of  $\text{CrCl}_3$ . STM topographs mix contributions from electronic states over a broad energy window and may therefore superimpose several moiré modulations of electronic origin. To overcome this limitation, we use tunneling spectroscopy to isolate the local density of states at a well-defined energy, enabling each moiré component to be individually identified in Fourier space. To this end, we performed scanning tunneling spectroscopy over a  $120 \text{ nm} \times 120 \text{ nm}$  region (STM topography in Figure 4a), where the  $\text{CrCl}_3$  lattice is twisted by  $31^\circ$  relative to the  $\langle 1\bar{1}0 \rangle_{\text{Au}}$  direction. Differential conductance ( $dI/dV$ ) maps were acquired across an energy range from  $-0.1 \text{ eV}$  to  $1.8 \text{ eV}$ . The FT of the  $dI/dV$  map at  $0.33 \text{ eV}$  (Figure 4c) reveals three sets of moiré spots, highlighted in green, red, and pink in Figure 4e. These results demonstrate that the moiré patterns in the  $\text{CrCl}_3^\beta$  islands manifest not only in topographic images but also in the spectroscopic  $dI/dV$  signal.

To examine how the spectral weight of each moiré component evolves with energy, we quantified the FT intensity at the corresponding moiré spot positions for each bias voltage. The resulting energy dependence is shown in Figure 4d. The spectral weights of the three moiré patterns vary strongly with energy. At  $0.33 \text{ eV}$ , the energy at which the FT in Figure 4e

was obtained, the pink moiré, originating from the conjunction of (6,1)CrCl<sub>3</sub> and (3,2)Au, dominates, despite being absent in the topographic channel. Each moiré pattern exhibits distinct resonances at specific energies, indicating a purely electronic origin. A similar conclusion was previously reached for CrCl<sub>3</sub><sup>α</sup> islands<sup>8</sup> where a single moiré was reported. In contrast, for the twisted CrCl<sub>3</sub><sup>β</sup> islands, multiple moiré components coexist, each displaying a distinct energy dependence, further reinforcing our interpretation of their purely electronic origin.

As a working hypothesis, we propose that when the wave vectors of the CrCl<sub>3</sub> electronic Bloch states match the moiré periodicity, a nesting-like effect may occur, leading to a spatial modulation of the electronic wave function. Density Functional Theory (DFT) calculations could provide further insight into this intriguing phenomenon. However, performing DFT calculations for this system is beyond the reach of the present study, primarily because the multiple coexisting moiré periods require an extremely large real-space supercell to be treated explicitly.

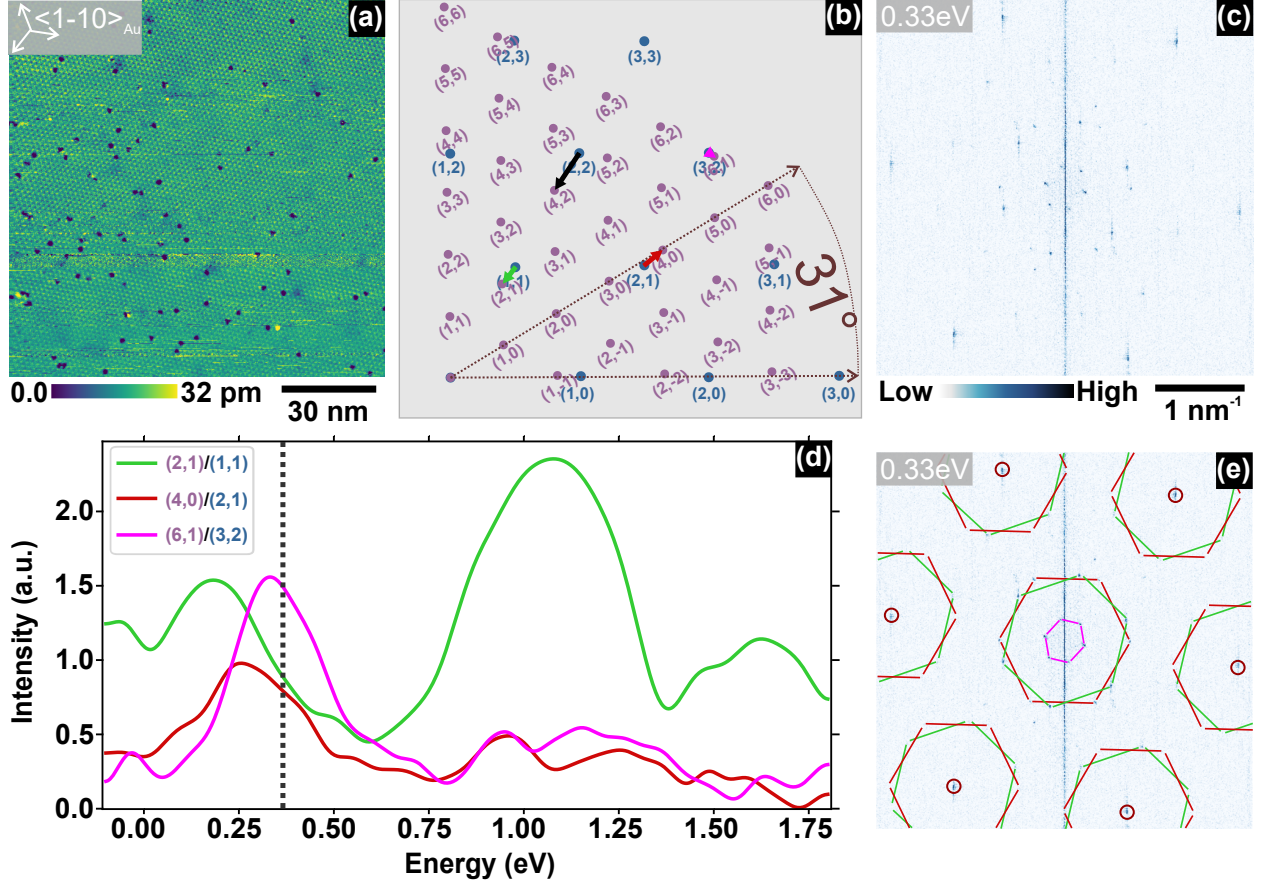


**Fig. 4.** (a) STM topography of  $31^\circ$  twisted  $\text{CrCl}_3\beta$  domain. Tunneling parameters:  $V = 1.8$  V,  $I = 200$  pA. (b) Reciprocal lattice construction of  $\text{CrCl}_3$  and Au. (c), (e) FT of dI/dV map at 0.33 eV, having distinct moiré components (green, red, pink). (d) Energy dependence of FT intensities extracted from the dI/dV maps for different moiré components.

To summarize, we investigated monolayer  $\text{CrCl}_3$  islands deposited on Au(111). The  $\text{CrCl}_3$  lattice is rotated by approximately  $30^\circ$  relative to the close-packed directions of Au(111). The incommensurability between  $\text{CrCl}_3$  and Au(111) lattices gives rise to a quasiperiodic pattern resulting from the superposition of several moiré orders. We show that multiple moirés can be observed directly for some orientations, and even when one appears dominantly in topography, additional moiré orders emerge in reciprocal space. Importantly, the spectral weight of these distinct moiré components varies considerably with electron energy, demonstrating that the observed quasiperiodic pattern arises from an electronic, rather than structural, modulation.

When simulating electronic or magnetic properties of moiré systems, it is quite generic to assume a single moiré periodicity in the form of a supercell. For instance, this results in the prediction of a non-collinear magnetic order with a well-defined period<sup>26</sup> that is driven by the considered moiré, considering additional moiré would certainly result in a more complex spin texture. Our results suggest that, in practice, multiple magnetic periods are likely to coexist. This would give rise to a quasiperiodic spin texture that could be probed by spin-resolved STM for instance. Similarly, in systems where mechanisms such as chiral topological superconductivity are associated with a specific moiré period,<sup>29</sup> it becomes natural to ask how the electronic properties evolve when additional moiré periodicities are considered. The coexistence of multiple moiré patterns may therefore lead to a richer and more complex phenomenology than previously anticipated.

## Experimental

All experiments were performed under ultra high vacuum (UHV) conditions. The Au(111) single crystal was cleaned by repeated cycles of argon-ion sputtering and annealing at 450 °C. Anhydrous CrCl<sub>3</sub> powder was carefully degassed prior to deposition and evaporated from a Knudsen cell onto the clean Au(111) surface at room temperature. To obtain flat CrCl<sub>3</sub> islands, the sample was subsequently annealed at 150 °C for a few minutes.

STM topography measurements were carried out at 4.2 K in UHV using electrochemically etched tungsten tips in both a home-built low temperature STM and a commercial Omicron LT-STM. Scanning tunneling spectroscopy (STS) measurements were performed in situ using the home-built setup. The tunneling setpoints were typically 200 pA and 1.8 V.

The spectroscopic grid (Figure 4) was recorded over an area of 120 nm × 120 nm, with the STM tip positioned every 234 pm to acquire an I(V) spectrum between −0.1 V and 1.8 V. Differential conductance curves (dI/dV) were obtained by numerical differentiation of the raw I(V) data. Individual dI/dV maps were extracted at each bias voltage and Fourier

transformed. The spectral weight of each moiré spot was then quantified as a function of the bias voltage.

## References

- (1) Zeller, P.; Günther, S. What are the possible moiré patterns of graphene on hexagonally packed surfaces? Universal solution for hexagonal coincidence lattices, derived by a geometric construction. *New Journal of Physics* **2014**, *16*, 083028, Publisher: IOP Publishing.
- (2) Loginova, E.; Nie, S.; Thürmer, K.; Bartelt, N. C.; McCarty, K. F. Defects of graphene on Ir(111): Rotational domains and ridges. *Physical Review B* **2009**, *80*, 085430, Publisher: American Physical Society.
- (3) Blanc, N.; Coraux, J.; Vo-Van, C.; N'Diaye, A. T.; Geaymond, O.; Renaud, G. Local deformations and incommensurability of high-quality epitaxial graphene on a weakly interacting transition metal. *Physical Review B* **2012**, *86*, 235439.
- (4) N'Diaye, A. T.; Coraux, J.; Plasa, T. N.; Busse, C.; Michely, T. Structure of epitaxial graphene on Ir(111). *New Journal of Physics* **2008**, *10*, 043033.
- (5) Merino, P.; Švec, M.; Pinardi, A. L.; Otero, G.; Martín-Gago, J. A. Strain-Driven Moiré Superstructures of Epitaxial Graphene on Transition Metal Surfaces. *ACS Nano* **2011**, *5*, 5627–5634, Publisher: American Chemical Society.
- (6) Krane, N.; Lotze, C.; Franke, K. J. Moiré structure of MoS<sub>2</sub> on Au(111): Local structural and electronic properties. *Surface Science* **2018**, *678*, 136–142.
- (7) Reidy, K.; Varnavides, G.; Thomsen, J. D.; Kumar, A.; Pham, T.; Blackburn, A. M.; Anikeeva, P.; Narang, P.; LeBeau, J. M.; Ross, F. M. Direct imaging and electronic

- structure modulation of moiré superlattices at the 2D/3D interface. *Nature Communications* **2021**, *12*, 1290, Publisher: Nature Publishing Group.
- (8) Gambari, E.; Meyer, S.; Guesne, S.; David, P.; Debontridder, F.; Limot, L.; Scheurer, F.; Brun, C.; Dupé, B.; Cren, T.; Hervé, M. Higher Order Topological Defects in a Moiré Lattice. *Advanced Functional Materials* **2024**, *34*, 2407438, \_eprint: <https://onlinelibrary.wiley.com/doi/pdf/10.1002/adfm.202407438>.
- (9) Li, G.; Luican, A.; Lopes dos Santos, J. M. B.; Castro Neto, A. H.; Reina, A.; Kong, J.; Andrei, E. Y. Observation of Van Hove singularities in twisted graphene layers. *Nature Physics* **2010**, *6*, 109–113, Publisher: Nature Publishing Group.
- (10) Cao, Y.; Fatemi, V.; Fang, S.; Watanabe, K.; Taniguchi, T.; Kaxiras, E.; Jarillo-Herrero, P. Unconventional superconductivity in magic-angle graphene superlattices. *Nature* **2018**, *556*, 43–50, Publisher: Nature Publishing Group.
- (11) Xie, H.; Luo, X.; Ye, Z.; Sun, Z.; Ye, G.; Sung, S. H.; Ge, H.; Yan, S.; Fu, Y.; Tian, S.; Lei, H.; Sun, K.; Hovden, R.; He, R.; Zhao, L. Evidence of non-collinear spin texture in magnetic moiré superlattices. *Nature Physics* **2023**, *19*, 1150–1155, Number: 8 Publisher: Nature Publishing Group.
- (12) Cheng, G.; Rahman, M. M.; Allcca, A. L.; Rustagi, A.; Liu, X.; Liu, L.; Fu, L.; Zhu, Y.; Mao, Z.; Watanabe, K.; Taniguchi, T.; Upadhyaya, P.; Chen, Y. P. Electrically tunable moiré magnetism in twisted double bilayers of chromium triiodide. *Nature Electronics* **2023**, *6*, 434–442, Number: 6 Publisher: Nature Publishing Group.
- (13) Song, T.; Sun, Q.-C.; Anderson, E.; Wang, C.; Qian, J.; Taniguchi, T.; Watanabe, K.; McGuire, M. A.; Stöhr, R.; Xiao, D.; Cao, T.; Wrachtrup, J.; Xu, X. Direct visualization of magnetic domains and moiré magnetism in twisted 2D magnets. *Science* **2021**, *374*, 1140–1144, Publisher: American Association for the Advancement of Science.

- (14) Guo, Y.; Pack, J.; Swann, J.; Holtzman, L.; Cothrine, M.; Watanabe, K.; Taniguchi, T.; Mandrus, D. G.; Barmak, K.; Hone, J.; Millis, A. J.; Pasupathy, A.; Dean, C. R. Superconductivity in 5.0° twisted bilayer WSe<sub>2</sub>. *Nature* **2025**, *637*, 839–845, Publisher: Nature Publishing Group.
- (15) Foutty, B. A.; Kometter, C. R.; Devakul, T.; Reddy, A. P.; Watanabe, K.; Taniguchi, T.; Fu, L.; Feldman, B. E. Mapping twist-tuned multiband topology in bilayer WSe<sub>2</sub>. *Science* **2024**, *384*, 343–347, Publisher: American Association for the Advancement of Science.
- (16) Li, H.; Li, S.; Regan, E. C.; Wang, D.; Zhao, W.; Kahn, S.; Yumigeta, K.; Blei, M.; Taniguchi, T.; Watanabe, K.; Tongay, S.; Zettl, A.; Crommie, M. F.; Wang, F. Imaging two-dimensional generalized Wigner crystals. *Nature* **2021**, *597*, 650–654, Publisher: Nature Publishing Group.
- (17) Balents, L.; Dean, C. R.; Efetov, D. K.; Young, A. F. Superconductivity and strong correlations in moiré flat bands. *Nature Physics* **2020**, *16*, 725–733, Publisher: Nature Publishing Group.
- (18) Li, H. et al. Imaging moiré flat bands in three-dimensional reconstructed WSe<sub>2</sub>/WS<sub>2</sub> superlattices. *Nature Materials* **2021**, *20*, 945–950, Publisher: Nature Publishing Group.
- (19) Langer, T.; Förster, D. F.; Busse, C.; Michely, T.; Pfñür, H.; Tegenkamp, C. Sheet plasmons in modulated graphene on Ir(111). *New Journal of Physics* **2011**, *13*, 053006.
- (20) Artaud, A.; Magaud, L.; Le Quang, T.; Guisset, V.; David, P.; Chapelier, C.; Coraux, J. Universal classification of twisted, strained and sheared graphene moiré superlattices. *Scientific Reports* **2016**, *6*, 25670, Publisher: Nature Publishing Group.
- (21) Yang, H.; Zhang, T.; Liu, M.; Liu, L.; Wu, X.; Wang, Y. Moiré Pattern Dislocation in Continuous Atomic Lattice of Monolayer h-BN. *ACS Applied Electronic Materials* **2022**, *4*, 891–896, Publisher: American Chemical Society.



- (22) Pham, T. T.; Vancsó, P.; Szendrő, M.; Palotás, K.; Castelino, R.; Bouatou, M.; Chacon, C.; Henrard, L.; Lagoute, J.; Sporken, R. Higher-indexed Moiré patterns and surface states of MoTe<sub>2</sub>/graphene heterostructure grown by molecular beam epitaxy. *npj 2D Materials and Applications* **2022**, *6*, 1–11, Publisher: Nature Publishing Group.
- (23) Günther, S.; Zeller, P.; Böller, B.; Wintterlin, J. Method for the Manual Analysis of Moiré Structures in STM images. *ChemPhysChem* **2021**, *22*, 870–884, \_eprint: <https://chemistry-europe.onlinelibrary.wiley.com/doi/pdf/10.1002/cphc.202001034>.
- (24) Hennighausen, Z.; Kar, S. Twistronics: a turning point in 2D quantum materials. *Electronic Structure* **2021**, *3*, 014004, Publisher: IOP Publishing.
- (25) Schwab, J.; Mangold, F.; Frank, B.; Davis, T. J.; Giessen, H. Skyrmion bag robustness in plasmonic bilayer and trilayer moiré superlattices. *Nanophotonics* **2025**, *14*, 3955–3964, Publisher: De Gruyter.
- (26) Fumega, A. O.; Lado, J. L. Moiré-driven multiferroic order in twisted CrCl<sub>3</sub>, CrBr<sub>3</sub> and CrI<sub>3</sub> bilayers. *2D Materials* **2023**, *10*, 025026, Publisher: IOP Publishing.
- (27) Zeller, P.; Dänhardt, S.; Gsell, S.; Schreck, M.; Wintterlin, J. Scalable synthesis of graphene on single crystal Ir(111) films. *Surface Science* **2012**, *606*, 1475–1480.
- (28) Ster, M. L.; Märkl, T.; Brown, S. A. Moiré patterns: a simple analytical model. *2D Materials* **2019**, *7*, 011005, Publisher: IOP Publishing.
- (29) Kezilebieke, S.; Vaño, V.; Huda, M. N.; Aapro, M.; Ganguli, S. C.; Liljeroth, P.; Lado, J. L. Moiré-Enabled Topological Superconductivity. *Nano Letters* **2022**, *22*, 328–333, PMID: 34978831.

## Acknowledgement

The authors thanks Pascal David for technical support. This work was supported by the French Agence Nationale de la Recherche through the contract ANR GINET2-0 (ANR-20-CE42-0011) and the ANR MASCOTE (ANR-24-CE30-1342). E.G. acknowledged the GDR-NS-CPU for funding it research stay in IPCMS.

## Supporting Information Available

The following file is available free of charge.

- Supporting Information